Available online at www.sciencedirect.com
ScienceDirect
Journal of Catalysis 242 (2006) 241–253
JOURNAL OF CATALYSIS
www.elsevier.com/locate/jcat

Fe-based perovskites substituted by copper and palladium for NO + CO reaction

Runduo Zhang [a], Houshang Alamdari [b], Serge Kaliaguine [a,*]

[a] *Department of Chemical Engineering, Laval University, Ste Foy (QC), G1K 7P4, Canada*
[b] *Nanox Inc., 4975 rue Rideau, Local 100, Quebec, G2E 5H5, Canada*

Received 10 March 2006; revised 25 May 2006; accepted 31 May 2006

Available online 17 July 2006

Abstract

Nanoscale Fe-based perovskites with nominal formula $LaFe_{1-x}(Cu,Pd)_xO_3$ were generated by reactive grinding and characterized by N_2 adsorption, X-ray diffraction (XRD), temperature-programmed reduction by hydrogen (H_2-TPR), temperature-programmed desorption (TPD) of O_2, NO, and CO, temperature-programmed surface reduction (TPSR) of NO under CO/He flow, and activity test toward NO + CO reaction. The catalytic performance of $LaFeO_3$ can be considerably improved via 20% Cu substitution, leading to a 74% N_2 yield and 72% CO conversion at 350 °C, under an atmosphere of 3000 ppm NO and 3000 ppm CO in helium at a space velocity of 50,000 h^{-1}. This improvement was ascribed to the facility in generation of anion vacancies after Cu incorporation, which plays a crucial role on NO adsorption and dissociation. In addition, the enhanced reducibility of $LaFe_{0.8}Cu_{0.2}O_3$ after Cu substitution results in the promotion of CO oxidation and anion vacancy regeneration, providing another clue for this improvement. N_2O decomposition (31% N_2 yield at 500 °C) is much easier than NO decomposition (below 5% at $T < 500$ °C) over $LaFe_{0.8}Cu_{0.2}O_3$. Conversion of both NO and N_2O is significantly improved by the presence of the reducing agent. A mechanism was proposed with dissociation of chemisorbed NO, forming N_2 and/or N_2O, and an oxidized perovskite surface, which was continuously reduced by CO with the generation of CO_2. Great performance at low temperature was found over $LaFe_{0.97}Pd_{0.03}O_3$ with a 96% NO conversion and 86% CO conversion at 300 °C, corresponding to the outstanding redox properties of this catalyst. O_2 has a strongly detrimental effect, leading to the consumption of the reducing agent by oxidation.

Keywords: NO reduction; Carbon monoxide; Reactive grinding; High surface area; Iron; Perovskite

1. Introduction

Perovskite-type oxides with the general formula ABO_3, where A usually stands for a rare earth metal cation coordinated by 12 oxygens and B usually designates a transition metal cation surrounded by six oxygens in octahedral coordination, exhibit interesting physicochemical properties. A great diversity of perovskites can be achieved by a careful adjustment of their compositions with different metal ions in A or B sites while satisfying the limit of tolerance factor $t = (r_A + r_O)/\sqrt{2}(r_B + r_O)$, where r_A, r_B, and r_O are the ionic radii for A, B, and O. Moreover, their physicochemical properties can be modified by partial substitution in A and/or B sites with metals of different oxidation states, which plays an important role in various redox reactions [1,2].

As long ago as 1952, perovskites were being used as catalytic materials for CO oxidation [3]. Twenty years later, their potential application as catalysts for automobile exhaust purification was pointed out by Libby [4]. Much attention has been paid in the last three decades to perovskites as candidates for NO reduction using CO as a reducing gas to simultaneously control the emission of those two pollutants from motor vehicles, with the studies focusing mainly on the following compositions: La(Fe, Mn)O_3 [5], $La_{1-x}Sr_xFeO_3$ [6], $La_{1-x-y}Sr_xCe_yFeO_3$ [7], La_2CuO_4 [8], La(Cr, Mn, Co, Ni)O_3 [8], and $LaCoO_3$ [9]. Copper and iron lanthanates were considered the most active among the lanthanum perovskites of the first transition element series in the

* Corresponding author. Fax: +1 418 656 3810.
E-mail address: kaliagui@gch.ulaval.ca (S. Kaliaguine).

0021-9517/$ – see front matter © 2006 Published by Elsevier Inc.
doi:10.1016/j.jcat.2006.05.033

CO + NO reaction according to the literature [10]. The activity of La_2CuO_4 for NO reduction with CO can be enhanced after Fe substitution by means of textural promotion of the dispersion of Cu^{2+} ions, as reported by Peter et al. [10]. A high reactivity of isolated copper in NO elimination was reported by Iwamoto [11] and confirmed by our early work [12–15]. Thus, good catalytic performance can be expected by means of evenly distributing Cu into lanthanum ferrite via B-site substitution.

Noble metal palladium is less expensive than Pt and Rh, has a good activity for the oxidation of hydrocarbons and carbon monoxide, and shows an excellent potentiality for NO elimination with no-rhodium catalysts [16–18]. It was found to be a suitable procedure to stabilize palladium against reaction with support and volatilization by incorporating Pd into a perovskite lattice. Substituted Pd can also move in and out of the perovskite framework, resulting in better resistance to sintering [17]. In addition, significantly enhanced activity of simple perovskites for NO removal was achieved from addition of even small amounts of palladium [16].

The use of perovskites synthesized by the traditional ceramic method was limited by their low BET surface areas, usually $<5\ m^2/g$ [19]. A new method of perovskite preparation, called reactive grinding, was developed by our group with the aim of improving the specific surface area while getting highly dispersed metal ions into the solid phase and also satisfying the requirements of several practical applications [20–23].

The objective of this work was to investigate the influence of substitution of trivalent Fe cation by divalent Cu or Pd cation on the physicochemical properties of lanthanum ferrite and to clarify the correlation between perovskite properties and their catalytic behavior in the NO + CO reaction. An attempt was also made to propose a mechanism for Fe-based perovskites. This work is therefore a continuation of our recently reported study of NO reduction by propene in the presence of oxygen over $LaFe_{1-x}(Cu, Pd)_xO_3$ catalysts [13].

2. Experimental

2.1. Preparation of perovskites

A series of $LaFe_{1-x}(Cu, Pd)_xO_3$ mixed oxides were prepared by reactive grinding. Powders of La_2O_3 (Alfa, 99.99%), Fe_2O_3 (Baker & Adamson, 97.49%), PdO (Aldrich, 99.98%), or CuO (Aldrich, 99%) were mixed in the desired proportions, then introduced into a vial with three tempered steel balls. The La_2O_3 powder was calcined at 600 °C for 24 h to transform any $La(OH)_3$ to La_2O_3 before grinding. The high-energy grinding was performed via a SPEX 800 shaker mill normally at a speed of 1100 rpm. This grinding process was conducted in two steps of 8 h for synthesis and 10 h for refining with ZnO as the grinding additive.

2.2. Characterization

2.2.1. BET surface area and pore size distribution

The specific surface area and pore size distribution of the samples calcined at 500 °C for 5 h were determined by nitrogen adsorption using an automated gas sorption system (NOVA 2000, Quantachrome). Before each measurement, the sample (about 200 mg) was degassed at 300 °C under vacuum until complete removal of humidity (approximately 6 h). The specific surface area was obtained from the linear part of the BET curve ($P/P_0 = 0.01$–0.10). The average pore diameter was calculated from the desorption branch of N_2 isotherms according to the Barrett–Joyner–Halenda (BJH) formula.

2.2.2. Elemental analysis

The chemical composition (Fe, Cu, and Pd) of the prepared solids and the residual impurity (Zn) were analyzed by atomic absorption spectroscopy (AAS) using a Perkin–Elmer 1100B spectrometer. The amount of La in solid solutions was established by inductively coupled plasma (ICP) spectrometry (Optima 4300DV, Perkin–Elmer). All materials were dissolved in a mixture of 10% HCl solution and concentrated HF at 60 °C for 24 h before elemental analysis.

2.2.3. Crystal phase identification and crystallite size analysis

The crystal structure of the prepared samples was determined by XRD using a Siemens D5000 diffractometer using Cu$K\alpha$ radiation ($\lambda = 1.5406$ Å) with step scans from 20 to 70° in a 2θ angle and 2.4 s for each 0.05° step. Particle sizes (D) were evaluated by means of the Scherrer equation after Warren's correction for instrumental broadening, $D = 0.9\lambda/(\sqrt{w_1^2 - w_0^2}\cos\theta)$, where λ is the incident wavelength, w_1 is the full width at half-maximum (FWHM) of X-ray reflection at $2\theta \approx 32°$, w_0 is the instrumental broadening determined through the FWHM of the X-ray reflection at $2\theta \approx 28°$ of SiO_2 with particles larger than 1 μm. Identification of the crystal phases was achieved via the JCPDS data bank.

2.2.4. Temperature-programmed analysis

Temperature-programmed reduction by hydrogen (H_2-TPR); temperature programmed desorption (TPD) of O_2, NO, and CO; and temperature-programmed surface reduction (TPSR) of NO under CO/He flow were performed using a multifunctional characterization system (RXM-100, ASD Inc.) equipped with a quadrupole mass spectrometer (MS) (UTI 100) and a thermal conductivity detector (TCD). Before H_2-TPR, the samples (50 mg) were pretreated under 10% O_2/He flow at a rate of 20 ml/min (STP) for 1 h at 500 °C, cooled to room temperature under the same atmosphere and purged by 20 ml/min helium for 40 min to remove the physisorbed O_2, then switched to a 5% H_2/Ar stream with the temperature rising up to 800 °C at a heating rate of 5 °C/min. The water in effluent gas of TPR process was condensed via a cold trap filled with a mixture of dry ice and ethanol. H_2 consumption was recorded continuously by TCD with 20 ml/min of 5% H_2/Ar as reference gas.

Before the TPD of O_2, NO, and CO, 50 mg samples were treated with the various atmospheres of 10% O_2, 3000 ppm NO, and 3000 ppm CO, respectively, with a total flow rate of

Table 1
Properties of $LaFe_{1-x}(Cu, Pd)_xO_3$ mixed oxides after calcination at 500 °C for 5 h

Sample	Chemical composition[a]	Specific surface area (m^2/g)	Pore diameter (nm)	Crystallite size (nm)	Crystal phase	Perovskite symmetry
$LaFeO_3$	$La_{0.99}Fe_{1.0}O_{3\pm\delta}$	30.5	16.2	18.7	$LaFeO_3/Fe_2O_3$[b]	Orthorhombic
$LaFe_{0.97}Pd_{0.03}O_3$	$La_{0.96}Fe_{0.97}Pd_{0.03}O_{3\pm\delta}$	48.1	11.8	18.9	$LaFeO_3$	Orthorhombic
$LaFe_{0.8}Cu_{0.2}O_3$	$La_{0.97}Fe_{0.80}Cu_{0.20}O_{3\pm\delta}$	41.6	14.6	16.8	$LaFeO_3$	Orthorhombic

[a] Zn can be detected as contaminant with a weight percent less than 2% of the total weight of Fe-based samples.
[b] Trace.

20 ml/min at 500 °C for 1 h and then cooled down to room temperature under the same atmosphere, subsequently, flushed by He as mentioned in H_2-TPR tests followed by heating the reactor up to 500 °C (800 °C for O_2-TPD) at a speed of 10 °C/min. O_2, NO, CO, and CO_2 desorbed during TPD experiments were monitored by on-line MS with mass numbers of 32, 30, 28, and 44, respectively. For ascription of mass 44 to either N_2O or CO_2, masses 30 and 12 were systematically monitored with ratios 30/44 or 12/44, allowing the ascription of mass 44 without ambiguity.

TPSR of NO under CO/He flow over $LaFe_{0.8}Cu_{0.2}O_3$ was performed with the same sample pretreatment as that for TPD of NO experiments. However, the thermodesorption was accomplished in 1000 ppm CO/He instead of He. The signals of desorbed N_2, O_2, NO, CO, and ($CO_2 + N_2O$) were recorded with the mass numbers of 14, 32, 30, 28, and 44, respectively. The gaseous responses obtained by MS or TCD were calibrated using standard gas mixtures.

2.3. Activity tests

The catalytic activity tests of about 100 mg $LaFe_{1-x}(Cu, Pd)_xO_3$ catalysts for CO + NO reaction were performed in a fixed-bed reactor under the mixture of 3000 ppm NO and 3000 ppm CO balanced by He at a total flow rate of 60 mL/min, corresponding to a gas hourly space velocity of 50,000 h^{-1}. In addition, the atmospheres of 3000 ppm N_2O + 3000 ppm CO, 3000 ppm NO, 3000 ppm N_2O, 3000 ppm CO, and 3000 ppm CO + 1500 ppm O_2 were also adopted for the reaction of N_2O + CO, NO or N_2O decomposition, and CO oxidation by perovskite or oxygen, respectively, over $LaFe_{0.8}Cu_{0.2}O_3$ at the same space velocity. The reactor was heated externally via a tubular furnace regulated by a temperature controller (Omega CN3240), via a thermocouple inserted in the catalyst bed, over the range of 100–500 °C in steps of 50 °C. Reactant and product content in the reactor effluent was recorded only after steady state was achieved at each temperature step. Nitrogen oxides (NO and NO_2) were analyzed using a chemiluminescence $NO/NO_2/NO_x$ analyzer (Model 200AH, API Inc.). N_2O and CO gases were monitored using a FTIR gas analyzer (FTLA 2000, ABB Inc.). N_2 was analyzed with a gas chromatograph (GC) (Hewlett Packard 5890) equipped with a TCD and columns of molecular 13X (45–60 mesh, 2.4 m) combined with Silicone OV-101 (100–120 mesh, 0.6 m) operating at an oven temperature of 30 °C. Calibration was done with a standard gas containing known concentrations of the components.

3. Results

3.1. Physicochemical properties

The chemical compositions of the prepared solids determined by AAS and ICP are close to the nominal values (Table 1). The BET specific surface areas and pore diameters of the materials prepared by reactive grinding are also reported in Table 1, showing a specific surface area approximately 30 m^2/g for the $LaFeO_3$ solid solution even after calcination at 500 °C. This value is enhanced after Pd or Cu substitution reaching values in excess of 40 m^2/g.

The crystal phase analysis was performed by XRD (not shown), revealing a main orthorhombic $LaFeO_3$ perovskite-type structure (JCPDS card 74-2203) for all prepared Fe-containing catalysts and small amounts of α-Fe_2O_3 (JCPDS card 86-0550) for the unsubstituted $LaFeO_3$ sample. No diffraction lines corresponding to PdO (JCPDS card 85-0713) or CuO (JCPDS card 80-1917) were observed, suggesting that Pd and Cu metals were fully incorporated into the $LaFeO_3$ structure or the formed particles of PdO and CuO were too tiny to be detected by XRD. The crystallite sizes were calculated using Scherrer's equation as given in Table 1, with values <20 nm. Based on the result that both pore diameters and crystallite sizes are around 10–20 nm, the porous structure of the present perovskites was believed to be realized via clustering of their individual nanoscale primary particles, in agreement with the literature [24].

3.2. Temperature-programmed reduction by hydrogen (H_2-TPR)

H_2-TPR experiments for the prepared perovskites were performed to investigate their reducibility; the results are shown in Fig. 1. A multiple-step reduction was observed over $LaFeO_3$, showing a small peak centered at 215 °C, followed by a broader peak and then a third intense one, fully overlapping, with maxima at 440 and 573 °C, respectively. After partial substitution of 3% Fe in lanthanum ferrite by Pd, H_2 consumption occurred at relatively low temperature (78 °C), followed by successive consumption at 219, 328, and 465 °C. The TPR profile of $LaFe_{0.8}Cu_{0.2}O_3$ exhibited one sharp reduction peak centered at 241 °C and another centered at 460 °C with shoulders at 360 and 550 °C.

Small amounts of highly reducible Fe^{4+} have been reported in $LaFeO_3$ [25–27], and its reduction to Fe^{3+} occurred at $T <$ 300 °C in H_2-TPR experiments [26]. Therefore, the minor reduction peak at 215 °C in the H_2-TPR profile of $LaFeO_3$ was

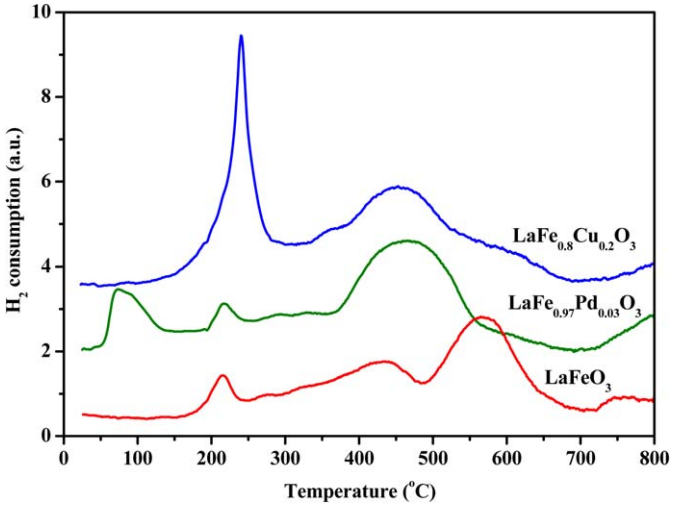

Fig. 1. H_2-TPR profiles of Fe-based perovskites [13].

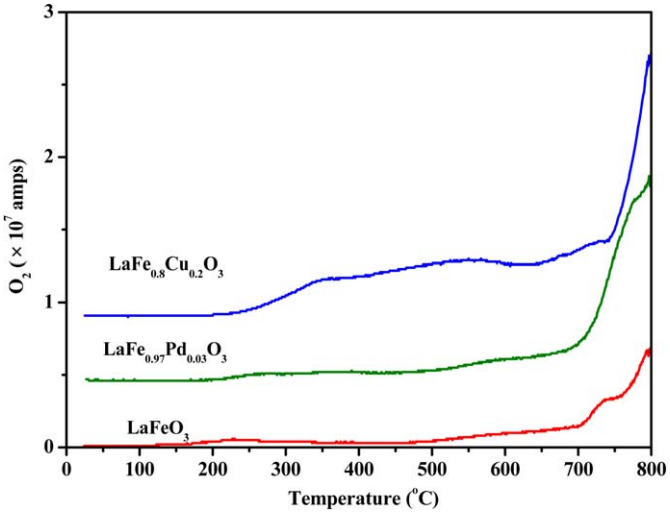

Fig. 2. TPD of O_2 profiles of Fe-based perovskites [13].

attributed to the reduction of Fe^{4+} to Fe^{3+}. The quantitative analysis of the successive Fe^{3+} reduction peaks with maxima at 440 and 573 °C correlated well with the H_2 consumption necessary for the reduction of Fe^{3+} to Fe^{2+}. Thus, those two peaks were ascribed to $Fe^{3+} \rightarrow Fe^{2+}$ reduction occurring over surface and in bulk of parent $LaFeO_3$, respectively. Finally, the minor reduction peak above 700 °C was ascribed to the partial reduction of Fe^{2+} to metallic iron. The low temperature (78 °C) H_2 consumption that occurs over $LaFe_{0.97}Pd_{0.03}O_3$, corresponds to the reduction of Pd^{2+} to Pd^0 according to the literature [28]. This result reveals the excellent redox properties of Pd-substituted perovskite, possibly leading to a good catalytic performance especially at low temperatures. $Fe^{4+} \rightarrow Fe^{3+}$ reduction is present at 219 °C, along with a downward shift of $Fe^{3+} \rightarrow Fe^{2+}$ reduction in the H_2-TPR profile of $LaFe_{0.97}Pd_{0.03}O_3$ with respect to that of $LaFeO_3$. This downward shift likely corresponds to the effect of atomic hydrogen generated on the Pd^0 already formed at this temperature level. The sharp peak at 241 °C observed in the H_2-TPR profile of Cu-substituted lanthanum ferrite was ascribed to the reduction of lattice Cu^{2+} to Cu^+, whereas the shoulder at 550 °C may be related to the complete reduction from Cu^+ to Cu^0. These values mostly coincide with those observed in H_2-TPR of Cu/MCM-41 [12], $LaCo_{1-x}Cu_xO_3$, and $LaMn_{1-x}Cu_xO_3$ ($x = 0.1, 0.2$) [14,15]. The Fe^{4+} reduction peak possibly overlaps with the rising part of the $Cu^{2+} \rightarrow Cu^+$ reduction peak, whereas the $Fe^{3+} \rightarrow Fe^{2+}$ reduction peak shifts to lower temperatures in Cu-substituted samples, suggesting that the lattice Cu^+ ions produced at this temperature interact with the iron ion, making it more easily reduced.

3.3. Temperature-programmed desorption of O_2, NO and CO (O_2, NO and CO-TPD)

The mobility of oxygen for Fe-based perovskites was investigated by O_2-TPD experiments, as illustrated in Fig. 2. The amount of O_2 released from perovskites was calculated after deconvolution of the O_2 desorption curve via Lorentzian peak fitting and reported in Table 2. The small amount of O_2 desorbed from $LaFeO_3$ at $T < 700$ °C is designated as α-O_2 and ascribed to oxygen species bound to the surface anion vacancies of perovskite [22]. More O_2 desorbed at $T > 700$ °C is referred to as β-O_2 and attributed to oxygen species liberated from the lattice [22]. Compared with $LaFeO_3$, similar α-O_2 desorption but more intense β-O_2 desorption was found over $LaFe_{0.97}Pd_{0.03}O_3$ during TPD of O_2. Interestingly, a broad plateau-like α-O_2 desorption peak at 200–700 °C together with a sharp β-O_2 peak maximum at 796 °C was observed in the O_2-TPD profile for $LaFe_{0.8}Cu_{0.2}O_3$ perovskite. This significant enhancement of adsorbed α-O_2 is likely related to the surface oxygen vacancies generated on Cu substitution.

Table 2
Amount of O_2 desorbed from Fe-based perovskites during O_2-TPD experiments

Sample	Amount of oxygen desorbed		
	α-O_2 (μmol/g) <700 °C	β-O_2 (μmol/g) 700–800 °C	Total (μmol/g)
$LaFeO_3$	38.2	76.2	114.4
$LaFe_{0.97}Pd_{0.03}O_3$	62.8	173.1	235.9
$LaFe_{0.8}Cu_{0.2}O_3$	196.5	202.2	398.7

Fig. 3 shows the desorption signals of NO ($m/e = 30$) during the NO-TPD process after the adsorption of 3000 ppm NO/He for the three Fe-based perovskites. The amount of NO desorbed from the perovskite was calculated after deconvolution and is given in Table 3. A minor desorption peak at 84 °C and an intense one centered at 214 °C with a slight shoulder at its falling part were observed in the NO desorption trace of $LaFeO_3$. Similar NO desorption behavior was found over Pd- and Cu-substituted perovskite except for an enhanced intensity of the second peak at approximately 220 °C. Low O_2 desorption parallel with only the high-temperature NO shoulder was observed during NO-TPD studies (not shown).

The MS signals of CO ($m/e = 28$) and CO_2 ($m/e = 44$) during the TPD of CO experiments over lanthanum ferrites were recorded. A quantitative analysis of the various carbonaceous gases desorbed from perovskites is presented in Table 4. CO

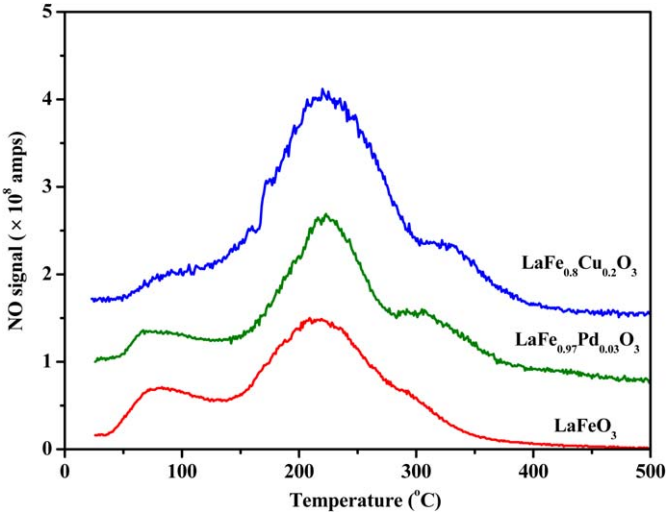

Fig. 3. TPD of NO profiles of Fe-based perovskites.

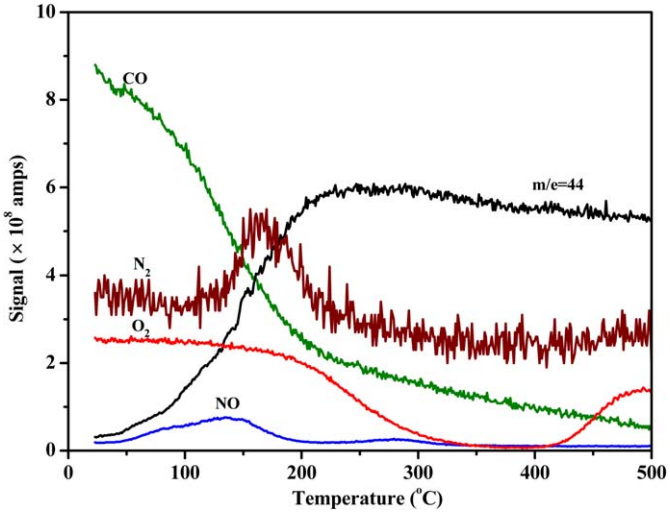

Fig. 4. MS signals during TPSR of NO under CO/He flow over $LaFe_{0.8}Cu_{0.2}O_3$ perovskite, conditions: flow rate = 20 ml/min, 3000 ppm NO, 1000 ppm CO.

Table 3
Amount of NO desorbed from Fe-based perovskites during NO-TPD experiments

	Physisorbed NO (μmol/g)	Chemisorbed NO (μmol/g)		
		Nitrosyl species	Nitrate species	Total
$LaFeO_3$	84 °C	214 °C	283 °C	22.0
	4.5	20.2	1.8	
$LaFe_{0.97}Pd_{0.03}O_3$	80 °C	222 °C	317 °C	27.1
	4.1	24.2	2.9	
$LaFe_{0.8}Cu_{0.2}O_3$	86 °C	225 °C	334 °C	39.6
	2.1	36.3	3.3	

Table 4
Amounts of CO and CO_2 desorbed from Fe-based perovskites during CO-TPD experiments

Sample	CO		CO_2		Total carbonaceous species
	T (°C)	Amount (μmol/g)	T (°C)	Amount (μmol/g)	Amount (μmol/g)
$LaFeO_3$	>250	53.2	>350	43.9	97.1
$LaFe_{0.97}Pd_{0.03}O_3$	>250	36.9	>200	102.5	139.4
$LaFe_{0.8}Cu_{0.2}O_3$	>225	25.0	>220	136.9	161.9

and CO_2 were desorbed from $LaFeO_3$ at temperatures above 250 and 350 °C, respectively. The CO desorption is gradually suppressed simultaneously with clearly enhanced CO_2 desorption after Pd or Cu incorporation into the B sites of $LaFeO_3$. This result implies that CO transformation into adsorbed CO_2 via oxidation over lanthanum ferrite is promoted by Pd or Cu substitution. The total carbonaceous species ($CO + CO_2$) desorbed from Fe-based perovskites follow the general trend of $LaFe_{0.8}Cu_{0.2}O_3 > LaFe_{0.97}Pd_{0.03}O_3 > LaFeO_3$.

3.4. Temperature-programmed surface reduction (TPSR) of NO under CO/He flow

TPSR of the NO profile measured under a flowing 1000 ppm CO/He mixture over $LaFe_{0.8}Cu_{0.2}O_3$ is depicted in Fig. 4. The oxygen signal detected by MS rapidly diminished over the range of 100–350 °C simultaneously with consumption of CO, whereas recovery of this O_2 signal occurred at $T > 400$ °C. At temperatures below 200 °C, the desorption peak of NO in Fig. 3 (2.1 μmol/g) appeared again in Fig. 4 (6.1 μmol/g) with a slight increase in density and a small upward shift. However, the NO thermodesorption peak centered at 225 °C (36.3 μmol/g) and the shoulder at its falling part (3.3 μmol/g) in Fig. 3 is totally suppressed in Fig. 4, leaving only a NO desorption of 0.7 μmol/g at about 280 °C. This result indicates that the corresponding adsorbed NO species almost entirely reacted with CO. Some N_2 desorption (4.9 μmol/g) with a maximum at 160 °C was indeed observed but not in amounts comparable with the content of desorbed NO reported for the same sample in Fig. 3. The appearance of mass 44, which could in this case be ascribed to both CO_2 and N_2O, coincided with the disappearance of CO.

3.5. Activity tests

A blank test was performed under 60 ml/min of 3000 ppm CO and 3000 ppm NO balanced by helium in an empty reactor (not shown). No significant NO conversion (<2%) or CO conversion (<5%) was observed up to 500 °C. Thus, the conversions generated from homogeneous reaction in the absence of catalyst are essentially negligible under usual reaction conditions. The temperature dependence of NO conversion over the three Fe-based perovskites is shown in Fig. 5a. Over unsubstituted $LaFeO_3$, the NO conversion became detectable at 250 °C and increased progressively with temperature, reaching 69% at 350 °C. An obvious enhancement was observed over lanthanum ferrite after Cu partial substitution, resulting in initiation at 200 °C and then reaching a value of 84% at 350 °C. NO conversion was 30% at 200 °C and up to 96% at 300 °C over $LaFe_{0.97}Pd_{0.03}O_3$. A similar order of $LaFe_{0.97}Pd_{0.03}O_3 > LaFe_{0.8}Cu_{0.2}O_3 > LaFeO_3$ for N_2 yield over perovskites was also observed (Fig. 5b). N_2O was detected in the effluent at low temperature, with a maximum yield of 13% at 300 °C over $LaFeO_3$, 16% at 300 °C over $LaFe_{0.8}Cu_{0.2}O_3$, and 41%

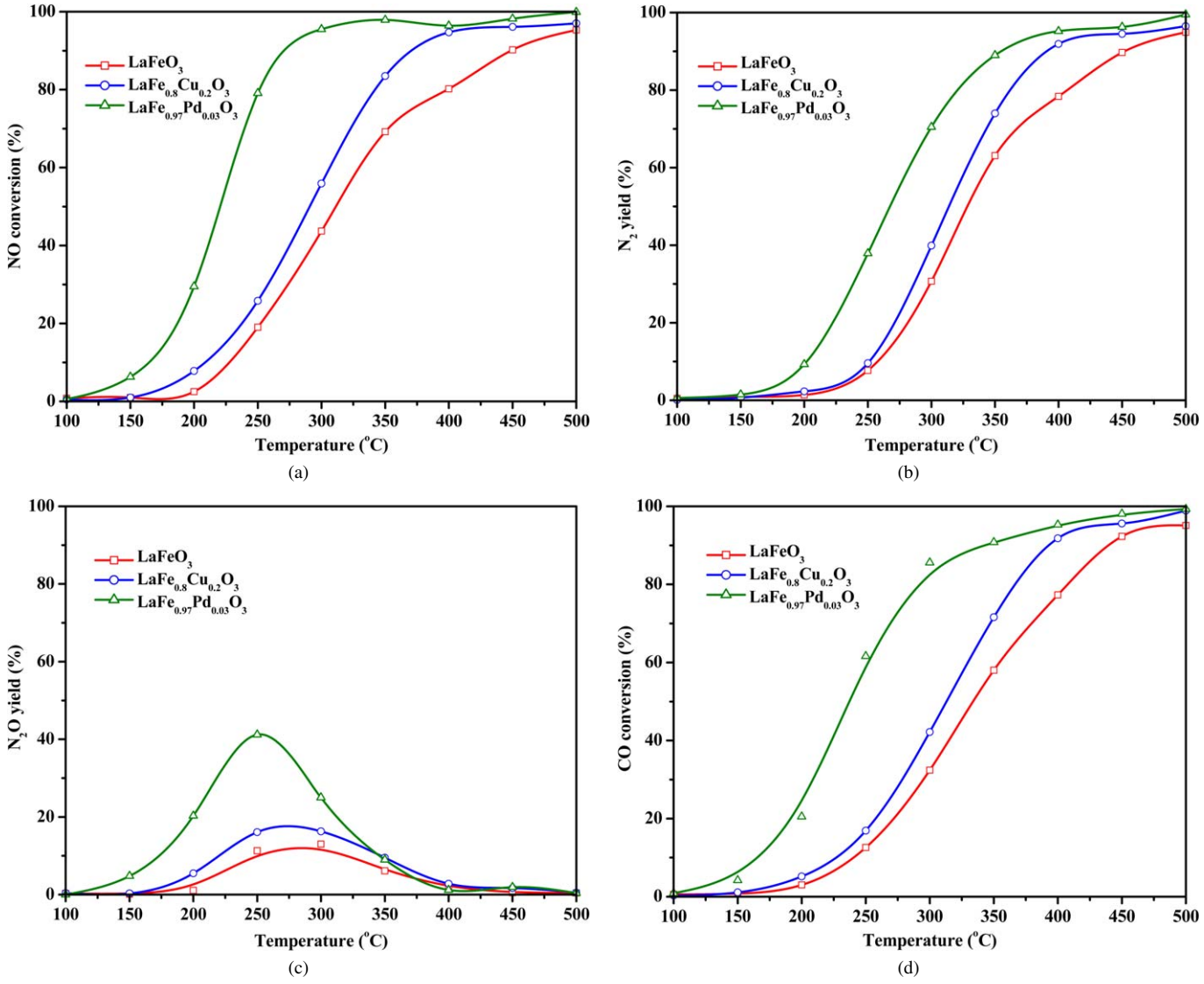

Fig. 5. (a) NO conversion in CO + NO reaction over Fe-based perovskites, conditions: GHSV = 50,000 h^{-1}, 3000 ppm NO, 3000 ppm CO. (b) N_2 yield in CO + NO reaction over Fe-based perovskites, conditions: GHSV = 50,000 h^{-1}, 3000 ppm NO, 3000 ppm CO. (c) N_2O yield in CO + NO reaction over Fe-based perovskites, conditions: GHSV = 50,000 h^{-1}, 3000 ppm NO, 3000 ppm CO. (d) CO conversion in CO + NO reaction over Fe-based perovskites, conditions: GHSV = 50,000 h^{-1}, 3000 ppm NO, 3000 ppm CO.

at 250 °C over $LaFe_{0.97}Pd_{0.03}O_3$, as depicted in Fig. 5c. The conversion of CO described in Fig. 5d showed a progressive increase up to 95% in the region of 200–500 °C for $LaFeO_3$. The conversion level was improved after Cu substitution, resulting in an increase from 32% to 42% at 300 °C compared with unsubstituted $LaFeO_3$. A remarkable CO conversion at low temperature was found over $LaFe_{0.97}Pd_{0.03}O_3$, achieving a conversion of 62% at temperature as low as 250 °C and reaching 86% at 300 °C.

N_2 yields in the reaction of NO + CO, N_2O + CO, NO decomposition, and N_2O decomposition for $LaFe_{0.8}Cu_{0.2}O_3$ are depicted in Fig. 6a. The objective of these experiments is a better understanding of NO and CO transformations in the catalytic process. In the absence of reducing agent, little NO decomposition (below 5%) was found at 350–500 °C. N_2O decomposition was much easier than NO decomposition starting at 350 °C and reached a N_2O conversion of 31% at 500 °C, likely related to the ease of its N–O bond cleavage. Nevertheless, it is noted that N_2O decomposition cannot occur at $T < 350$ °C, indicating that sufficient energy is still necessary for the dissociation of this N–O bond. The transformation of nitrogen oxides (NO and N_2O) into N_2 was significantly improved by CO as a reducing agent, resulting in N_2 yields of 40% in NO + CO reaction and 70% in N_2O + CO reaction at 300 °C. The higher N_2 yield in N_2O reduction by CO is again attributed to the facility of N_2O molecular activation compared with NO.

CO conversions in the reaction of NO + CO, N_2O + CO, CO oxidation by perovskite (no oxygen), and CO + O_2 over $LaFe_{0.8}Cu_{0.2}O_3$ are compared in Fig. 6b. CO oxidation can still occur with a maximum conversion of 40% at 450 °C in the absence of O_2, which is likely realized by consuming oxygen species from the perovskite surface. With the diminution of the remaining O_2 species by previous CO oxidation and by

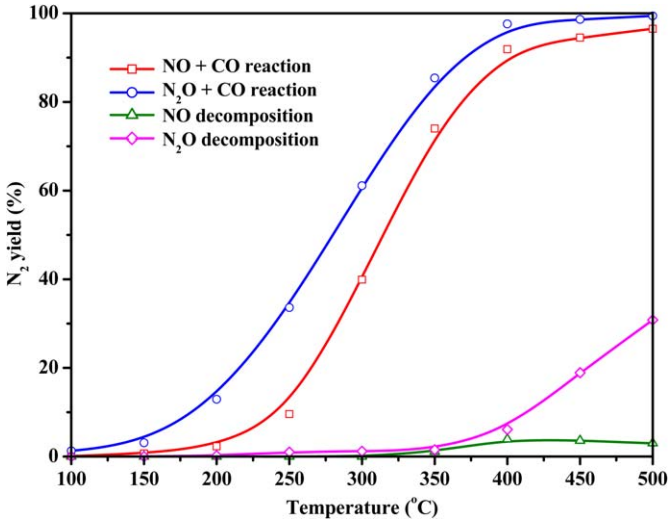

(a)

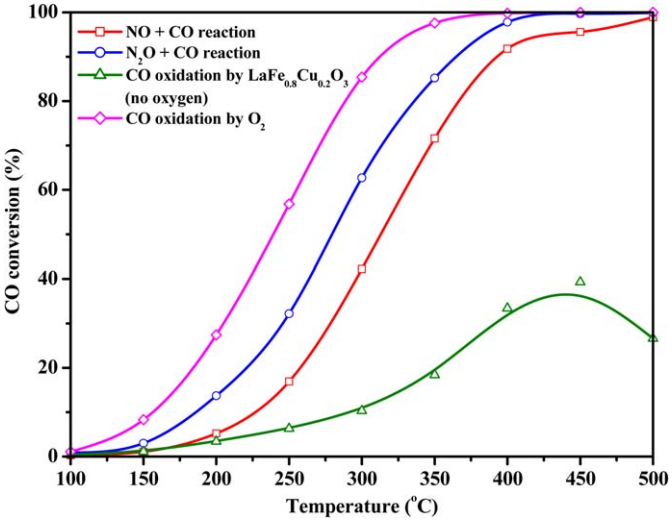

(b)

Fig. 6. (a) N_2 yield in various reactions over $LaFe_{0.8}Cu_{0.2}O_3$, conditions: GHSV = 50,000 h^{-1}, 3000 ppm NO, 3000 ppm N_2O, 3000 ppm CO. (b) CO conversion in various reactions over $LaFe_{0.8}Cu_{0.2}O_3$, conditions: GHSV = 50,000 h^{-1}, 3000 ppm NO, 3000 ppm N_2O, 3000 ppm CO, 1500 ppm O_2.

rapid O_2 desorption at relatively higher temperature, a decline in CO oxidation occurred. This rapid desorption of O_2 species at relatively higher temperature was indeed confirmed by O_2-TPD (Fig. 2) and TPSR (Fig. 4) studies. Nitrogen oxides (NO and N_2O) promoted CO oxidation of up to 42% and 72% at 300 °C, respectively. N_2O was again more active than NO in donating its oxygen atom and oxidizing CO. Gaseous oxygen with the same atomic O concentration as 3000 ppm NO or N_2O led to the highest CO oxidation, achieving a value of 85% even at 300 °C. The results, shown in Fig. 6b, suggest an order of the efficiency in oxygen utilization for CO oxidation as adsorbed oxygen molecule (O_2^-) > oxygen atom (O) in NO or N_2O > lattice oxygen (O^- or O^{2-}).

The influence of O_2 feed concentration on the catalytic performance of $LaFe_{0.8}Cu_{0.2}O_3$ is presented in Figs. 7a–7d to clarify the role of gaseous O_2 in NO + CO reaction. It is observed that the N_2 production obtained in the absence of O_2 was approximately twice its value in the presence of 500 ppm O_2. The introduction of 5% O_2 gas in feed led to a total inhibition of N_2 yield (Fig. 7a). N_2O concentration in effluent severely declined with an increase in O_2 feed concentration (Fig. 7b). NO_2 production was negligible during the reaction of 3000 ppm NO and 3000 ppm CO in the absence of O_2 and increased in its presence (Fig. 7c). CO conversion was indeed also promoted with increasing O_2 concentration in feed (Fig. 7d).

4. Discussion

4.1. O_2-TPD study

TPD of O_2 experiments were carried out to study the O_2 species formed over Fe-based perovskites after O_2 adsorption; the results are reported in Fig. 2 and Table 2. Among three Fe-containing samples, the lowest α- and β-O_2 desorptions were observed for $LaFeO_3$, revealing its low coverage of molecular oxygen and poor reducibility of lattice oxygen, in accordance with previous reports [29,30]. β-O_2 desorption of lanthanum ferrite can be significantly enhanced via substitution of just 3% Fe^{3+} in the B sites by Pd^{2+}, likely attributed to the improved mobility of lattice oxygen due to highly reducible Pd^{2+}, as proven by H_2-TPR analysis for $LaFe_{0.97}Pd_{0.03}O_3$ (Fig. 1). With the substitution of 20% Fe^{3+} by Cu^{2+}, significantly enhanced α-O_2 was achieved, ascribed to the generation of a positive charge deficiency after incorporation of Cu into the lattice, which is compensated for by oxygen vacancies. A similar enhancement in β-oxygen desorption by Cu substitution as by Pd substitution was also found and attributed to the improvement of lattice oxygen mobility according to the H_2-TPR trace for $LaFe_{0.8}Cu_{0.2}O_3$ (Fig. 1).

Based on our previous description [22], the following process was assumed to occur during calcination of $LaFeO_3$ perovskite:

1) Transient generation of anion vacancy during calcination of fresh sample

$$\mathrm{Fe^{3+}(OH)} + \mathrm{Fe^{3+}(OH)} \xrightarrow{-H_2O} \underset{\text{(anion vacancy)}}{\mathrm{Fe^{2+}\square}} + \mathrm{Fe^{3+}(O^-)}. \quad (1)$$

2) Instantaneous formation of α-O_2 by adsorbing O_2 at anion vacancy

$$\mathrm{Fe^{2+}\square} + O_2 \longrightarrow \mathrm{Fe^{3+}(O_2^-)}. \quad (2)$$

The following two reactions are proposed for the α-O_2 desorption process:

$$\mathrm{Fe^{3+}(O_2^-)} + \mathrm{Fe^{3+}(O^-)} \longrightarrow \mathrm{Fe^{3+}(O^{2-})Fe^{3+}} + O_2, \quad (3)$$

$$\mathrm{Fe^{3+}(O_2^-)} \longrightarrow \mathrm{Fe^{2+}\square} + O_2. \quad (4)$$

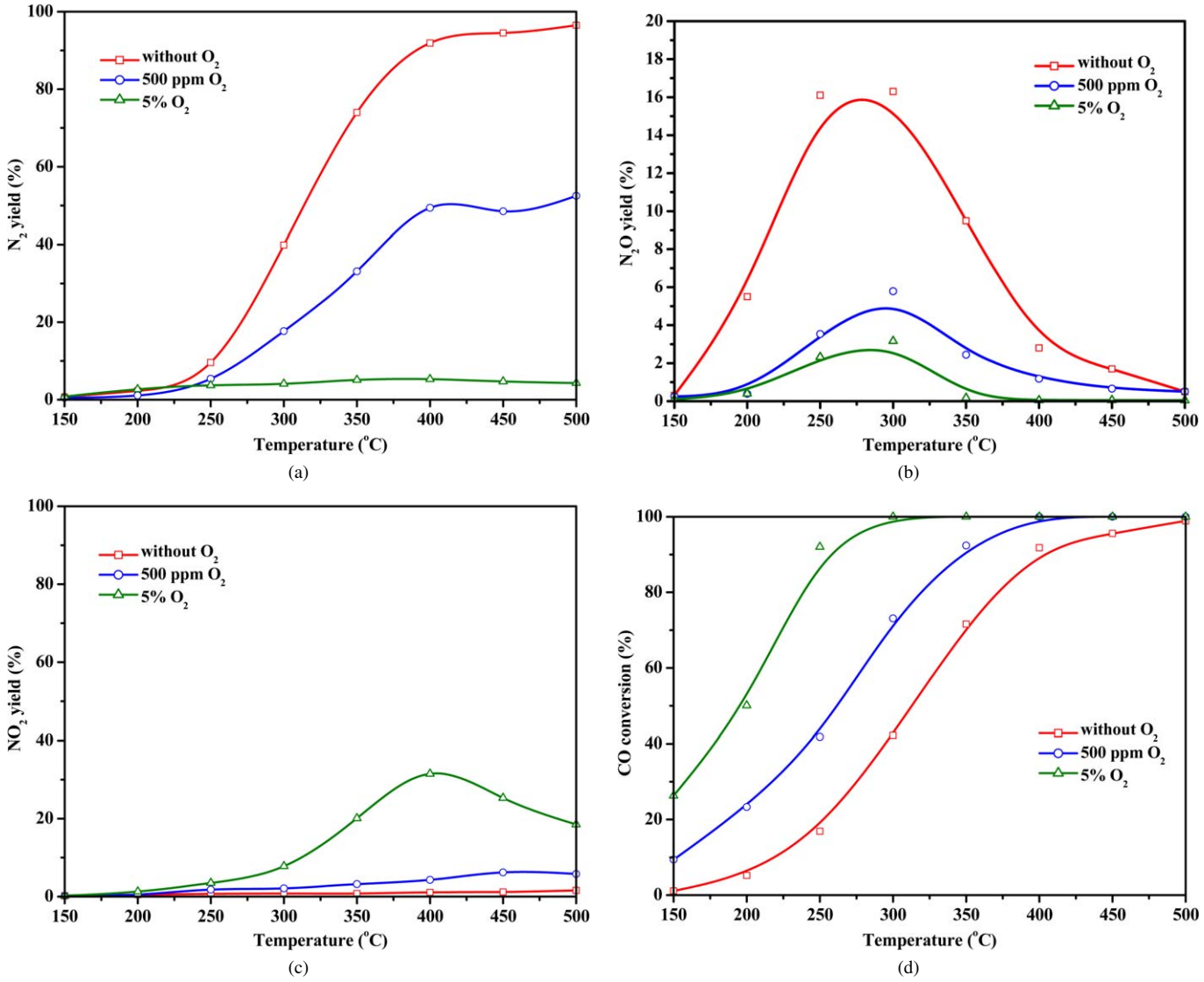

Fig. 7. (a) Effect of O_2 on N_2 yield in CO + NO reaction over $LaFe_{0.8}Cu_{0.2}O_3$ perovskite, conditions: GHSV = 50,000 h^{-1}, 3000 ppm NO, 3000 ppm CO, 0, 500 ppm, 5% O_2. (b) Effect of O_2 on N_2O yield in CO + NO reaction over $LaFe_{0.8}Cu_{0.2}O_3$ perovskite, conditions: GHSV = 50,000 h^{-1}, 3000 ppm NO, 3000 ppm CO, 0, 500 ppm, 5% O_2. (c) Effect of O_2 on NO_2 yield in CO + NO reaction over $LaFe_{0.8}Cu_{0.2}O_3$ perovskite, conditions: GHSV = 50,000 h^{-1}, 3000 ppm NO, 3000 ppm CO, 0, 500 ppm, 5% O_2. (d) Effect of O_2 on CO conversion in CO + NO reaction over $LaFe_{0.8}Cu_{0.2}O_3$ perovskite, conditions: GHSV = 50,000 h^{-1}, 3000 ppm NO, 3000 ppm CO, 0, 500 ppm, 5% O_2.

In Eqs. (1)–(4) iron ions are indicated as examples. In the substituted samples, pairs of one Fe^{3+} and one Cu^{2+} or Pd^{2+} are also present. Therefore, reactions (1) and (3) may occur on these new ion pairs. Processes (2) and (4) also occur in the coordination sphere of copper or palladium ions.

The oxygen desorbed above 700 °C was assigned as the β-oxygen liberated from the lattice leaving bulk oxygen vacancies and reduced cations. All of the steps for its desorption were described in our previous study on similar compounds [13].

4.2. NO-TPD study

The formation of (mono-, di-) nitrosyl and (monodentate, bidentate, bridging) nitrate species was found over $LaFeO_3$ [31], Cu/ZSM-5 [32], and Cu/MCM-41 [12] after NO adsorption as reported in the literature. In the present work, adsorbed N-containing species formed during NO adsorption over Fe-based perovskites were investigated by means of monitoring the NO desorption traces ($m/e = 30$) in the effluents by MS (Fig. 3). The amount of NO species desorbed was subsequently quantified, as given in Table 3. A broad NO desorption peak occurred at 210–230 °C with minor shoulders at the rising and falling parts, respectively, during NO-TPD experiments. Centi and Perathoner [33] concluded that the thermal stability of adsorbed species increased with increasing the oxidation state of nitrogen in N-containing adspecies according to transient catalytic experiments conducted over Cu/ZSM-5. In our previous NO + O_2-TPD studies over Co-, Mn-, and Fe-based perovskites [13–15], three NO peaks appearing at similar temperatures as those in the present NO-TPD experiments, apart from minor desorption at medium temperature and an intensive one at high temperature, were also found and ascribed to the desorption

of physisorbed NO, nitrosyl species, and nitrate species according to their thermal stability. The NO peaks obtained at low (80–90 °C), medium (210–230 °C), and high (280–340 °C) temperatures in present NO-TPD analyses were thus correlated to physisorbed NO, nitrosyl, and nitrate species, respectively.

O_2 desorption parallel with the minor NO desorption occurring at 283 °C for $LaFeO_3$ (not shown) gives another clue to the ascription of nitrate species in agreement with the report that the desorption of NO_3^- species would appear as a NO desorption peak at high temperature ($T > 300$ °C) associated with O_2 desorption [13–15,34,35]. It is noticeable that only a minor nitrate species was formed over perovskites after NO adsorption, appearing as a shoulder rather than as a peak with respect to nitrosyl species, although its density was slightly enhanced on Cu or Pd substitution.

Fig. 3 shows that the intensity of the broad NO peak at 214 °C for $LaFeO_3$ was enhanced via Pd and Cu substitution. Based on the fact that more oxygen vacancies can be generated after trivalent iron ions substituted by bivalent palladium or copper ions (as confirmed by O_2-TPD experiments (Fig. 2)), this intense NO desorption related to nitrosyl species was likely formed by NO adsorption on anion vacancies, as verified by Shin et al. via FTIR study [36]. The NO is chemisorbed as a negatively charged form (NO^-), which is thought to be the first important step for NO + CO reaction [37], because back-donation occurs through antibonding orbitals and thus determines a weakening of the N–O bond with a net electron transfer from metal to NO. The formation of nitrosyl species is formulated on the basis of the above discussion:

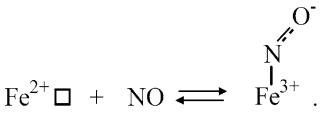

(5)

4.3. CO-TPD study

Tascón et al. [38] pointed out an inhibiting effect of NO on subsequent CO adsorption, which was greater than the inhibiting effect of CO on NO adsorption over $LaFeO_3$. Therefore, CO absorption appears to be weaker than NO absorption on the same site of Fe-based perovskites. The CO adsorption thus likely involves adsorption at anion vacancies with a coordinative bond without electron transfer:

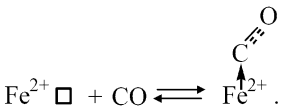

(6)

A decline in CO desorption and an opposite tendency in CO_2 desorption from Pd- or Cu-substituted samples compared with those from parent $LaFeO_3$ (Table 4) were observed, suggesting that CO oxidation occurred over Fe-based perovskites and was further improved by divalent cation substitution. The oxidation of CO has been suggested by Voorhoeve [39] to be a suprafacial catalytic process involving a surface lattice oxygen (O^-). Thus, CO oxidation was proposed as the following step:

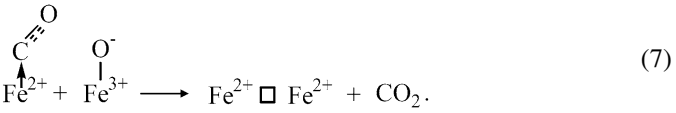

(7)

Furthermore, the lower binding energy for this surface lattice oxygen is favorable for CO oxidation [40]. The improved CO oxidation after Pd and Cu substitution can be explained by the enhanced mobility of the lattice oxygen, which was confirmed by H_2-TPR test in the present study (Fig. 1):

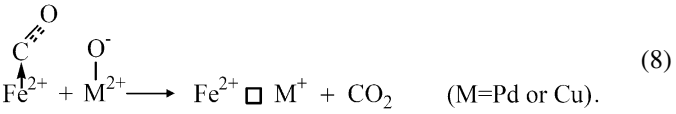

(8)

In the presence of O_2, this CO oxidation can be significantly accelerated by α-O_2 [40]:

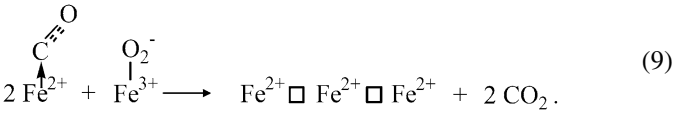

(9)

A higher content of adsorbed carbonaceous species was found over Cu- or Pd-substituted samples with respect to lanthanum ferrite, likely related to the enhanced density of anion vacancies (the adsorption sites for CO and O_2) after substitution.

4.4. TPSR of NO under CO/He flow

Fig. 4 shows that NO desorption related to nitrosyl species (observed at 225 °C in the NO-TPD profile of $LaFe_{0.8}Cu_{0.2}O_3$ in Fig. 3) almost vanishes in the presence of CO. Only the peak at low temperature, which was ascribed to physisorbed NO, is still significant in the NO desorption trace. This result implies that both nitrosyl and nitrate species are reactive toward CO and fully consumed by this reducing agent, in agreement with the previous conclusion that the chemisorption of NO seems to play an important role in the NO + CO reaction catalyzed by perovskites [41]. Nitrate species were proven to be highly active toward propene over perovskites [13–15] and toward methane over Ag/Al_2O_3 [34] and Ag-ZSM-5 [42], resulting in good $deNO_x$ activity at high temperature. The reactivity of this nitrate species toward CO was confirmed again in the present TPSR study. Nevertheless, the nitrate species formed over perovskites was minor (3.3 μmol/g) compared with the nitrosyl species (36.3 μmol/g) according to the NO-TPD study. Furthermore, NO reduction was already remarkable at $T < 300$ °C (Fig. 5a), whereas nitrate species seemed to be stable over this temperature range and corresponded only to high-temperature $deNO_x$ activity. Hence, nitrosyl species is believed to make the most significant contribution to NO reduction by CO.

Simultaneously with the CO consumption and $CO_2 + N_2O$ ($m/e = 44$) formation, the MS signal of O_2 decreased progressively in the range of 100–400 °C due to rapid CO oxidation. Nevertheless, recovery of the O_2 signal was obtained at $T > 400$ °C, likely related to rapid desorption of O_2 species at relatively high temperature. The O_2 consumption by CO to CO_2

oxidation was also slightly inhibited (see the $m/e = 44$ trace in Fig. 4), possibly due to a serious surface coverage of carbonate species, providing another explanation for these phenomena.

N_2 was also detected during this experiment, again suggesting that the reduction of nitrosyl species by CO is associated with the NO catalytic elimination.

4.5. Activity tests and reaction mechanism

The direct decomposition of NO would represent the most attractive solution in NO emission control, because no additional reactant was required for the reaction with potential products of only N_2 and O_2. In principle, simple NO decomposition is a thermodynamically favored reaction at low temperature; however, this reaction is very slow, due to the high dissociation energy of NO (153.3 kcal/mol), and sufficiently efficient catalysts have not yet been discovered [36]. Up to now, Cu-zeolites have been considered the best catalysts, with isolated Cu^+ ions considered as active centers in NO decomposition [11]. Perovskites exhibit better activity than most other metal oxides for this reaction, but at 500 °C they are still much less active than the best copper zeolites [43–45]. The fact that NO hardly decomposes over $LaFe_{0.8}Cu_{0.2}O_3$ perovskite at <500 °C was confirmed again in this work (Fig. 6a).

N_2O is not toxic, but it does play a role in ozone depletion. Its decomposition over $LaFe_{0.8}Cu_{0.2}O_3$ was examined, and the results (shown in Fig. 6a) demonstrated better activity in terms of N_2 yield (31% at 500 °C) than that achieved in NO decomposition (3% at 500 °C). N_2O is known to have a linear structure N–N–O, in which the N–O distance is increased by about 0.03 Å relative to free NO with a bond order of 2.5, resulting in an easy cleavage of its N–O bond and better dissociation behavior compared with NO. However, sufficient energy is still necessary for N–O bond breakage, according to the result that N_2O was merely decomposed at temperatures above 350 °C (Fig. 6a).

With the assistance of CO, N_2 yields for both NO and N_2O transformations were significantly improved, up to 74% in NO + CO reaction and 89% in N_2O + CO reaction even at 350 °C (Fig. 6a). Chien et al. [41] observed a higher NO adsorption rate for activated (reduced) than for unactivated $LaCoO_3$ and $La_{0.85}Ba_{0.15}CoO_3$. A reduced perovskite surface with large amount of anion vacancies was reported to be crucial for the NO dissociation according to FTIR and EPR spectroscopic analyses [46]; thus, the role of CO seems to be to maintain a reduced surface, which is necessary for successive NO dissociation. CO oxidation can also be promoted by the O atom coming from NO or N_2O (Fig. 6b) via a catalytic process. The above results and discussions indicate that these perovskites likely act as "oxygen reservoirs," transferring oxygen atoms from nitrogen oxides to CO and thus achieving NO reduction and CO oxidation simultaneously.

The high reactivity of nitrosyl species toward CO over $LaFe_{0.8}Cu_{0.2}O_3$ was established via TPSR of NO under a CO/He flow test. N_2O formation for this catalyst was observed during NO reduction by CO with a maximum yield of 16% at 300 °C and ultimately diminishing at higher temperature (Fig. 5c). Based on our previous studies and the present work, a mechanism for NO + CO reaction, including the adsorption and transformation of reactants over perovskite and redox catalytic recycling during reaction, with the product components depending on reaction temperature, was proposed that involves the following steps:

At low temperature, adsorbed nitrosyl species combine to yield adsorbed N_2O_2 species. This can decompose over the reduced perovskite, yielding N_2O and N_2 simultaneously with oxidation of the perovskite surface. The latter was recognized as a rate-determining step for NO reduction by CO at low temperature. The formation of the dimeric NO species (N_2O_2) involving the N–N bond formation is followed by N–O bond cleavage [47,48]. Two parallel reactions for chemisorbed NO dissociation thus occur over a reduced surface with N_2O and N_2 as the respective products:

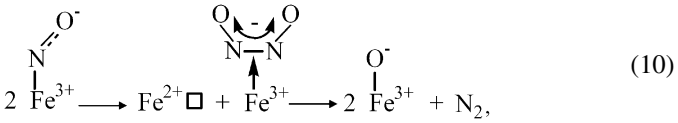

(10)

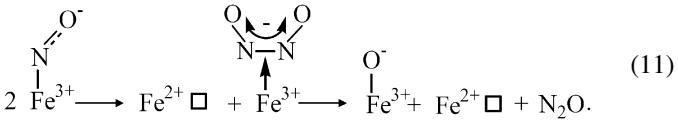

(11)

Reaction (11) involves the breakage of only one N–O bond, making this reaction occur much more easily than reaction (10), indicating that reaction (11) is dominating at low temperature. The above two reactions can also proceed on copper and palladium cations. CO can be oxidized by $Fe^{3+}O^-$ species, as illustrated in Eq. (7), together with regeneration of anion vacancies on the surface for the continuous NO dissociation.

The reaction routes occurring at low temperature can thus be described as two parallel reactions:

$$\text{Route (a):}\quad 2NO + 2CO \rightarrow N_2 + 2CO_2 \tag{12}$$

and

$$\text{Route (b):}\quad 2NO + CO \rightarrow N_2O + CO_2 \text{ (fast).} \tag{13}$$

Although N_2O is detected in the effluent as a byproduct at low temperature (see Fig. 5c), its further conversion as an intermediate must not be excluded [29,46,49]. Pomonis proposed a partially successive N_2O decomposition [Route (c): $2N_2O \rightarrow 2N_2 + O_2$], occurring at low temperature simultaneously with reaction (13) over $La_{1-x}Sr_xFeO_3$ [5,6,50] and $LaMnO_3$ [5]. However, N_2O decomposition was found to be quite difficult at <350 °C $LaFe_{0.8}Cu_{0.2}O_3$ (see the line for N_2O decomposition in Fig. 6a) and is believed to occur only over a reduced perovskite with the participation of CO to consume surface oxygen species (Fig. 6a):

$$\text{Route (d):}\quad N_2O + CO \rightarrow N_2 + CO_2. \tag{14}$$

The ratio of NO conversion to CO conversion must be equal to unity for Route (a) and to 2 for Route (b), whereas the molar ratio $[CO_2]/([N_2] + [N_2O])$ in the products should be 2 for Route (a) and 1 for Route (b) according to Eqs. (12) and (13).

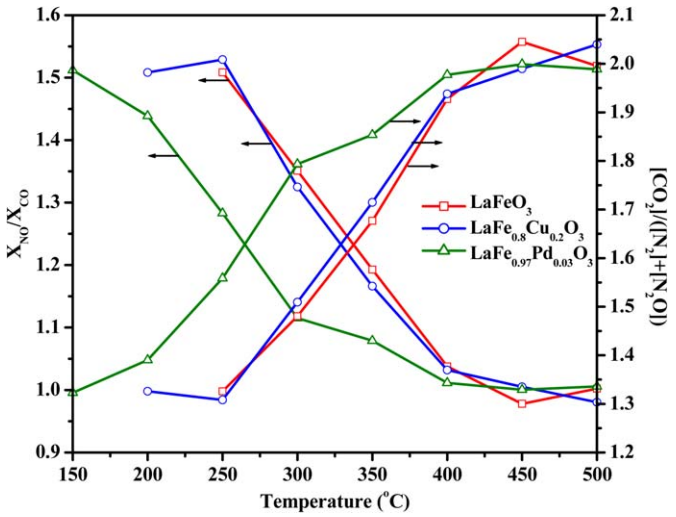

Fig. 8. Molar ratios of X_{NO}/X_{CO} and $[CO_2]/([N_2] + [N_2O])$ in CO + NO reaction over Fe-based perovskites, conditions: GHSV = 50,000 h^{-1}, 3000 ppm NO, 3000 ppm CO.

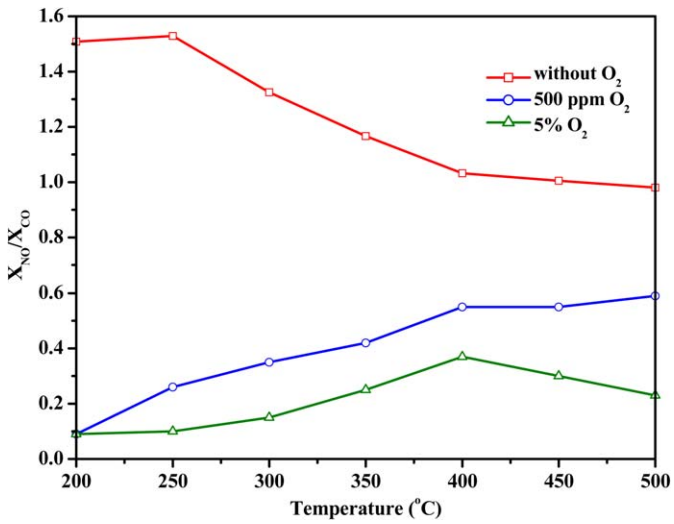

Fig. 9. O_2 effect on ratio of NO conversion to CO conversion in CO + NO reaction over $LaFe_{0.8}Cu_{0.2}O_3$ perovskite, conditions: GHSV = 50,000 h^{-1}, 3000 ppm NO, 3000 ppm CO, 0, 500 ppm, 5% O_2.

Therefore, the plots of X_{NO}/X_{CO} as well as $[CO_2]/([N_2] + [N_2O])$ versus temperature provide an easy way to probe the reaction route involved. X_{NO}/X_{CO} values of approximately 1.5 at low temperatures and 1 at $T > 400\,^{\circ}C$ for lanthanum ferrites were observed in the present study; moreover, the ratios of $[CO_2]/([N_2] + [N_2O])$ for these catalysts are close to 1.3 at low temperatures and 2 at $T > 400\,^{\circ}C$, as depicted in Fig. 8.

The reaction between CO and N_2O [Route (d)], as well as the decomposition of N_2O [Route (c)], were accelerated at rising temperature, as illustrated in Fig. 6a. As a result, all N_2O generated during NO dissociation could be rapidly consumed, and the reaction occurring at high temperature can be simplified as Route (a) with $X_{NO}/X_{CO} = 1$ and $[CO_2]/([N_2] + [N_2O]) = 2$.

The above analysis may be interpreted as more evidence supporting a mechanism dominated by Route (b) at low temperature and then gradually progressing to Route (a) at elevated temperature.

A significant improvement in N_2 yield was achieved after the incorporation of Cu into the B sites of Fe-based perovskite. Besides the essential effect of copper ions in the transformation of nitrogen oxides [33], Cu substitution promoted the generation of anion vacancies, which facilitated the adsorption of reactants (confirmed in NO-TPD (Fig. 3) and CO-TPD experiments (Table 4)), as well as the dissociation of adsorbed NO. In addition, the regeneration of anion vacancies was also accelerated after incorporation of Cu (see Eq. (8)) due to enhanced mobility of lattice oxygen. At low temperature, outstanding catalytic performance was found over $LaFe_{0.97}Pd_{0.03}O_3$ (Figs. 5a–5d), yielding NO conversion of 96% and CO conversion of 86% at temperature as low as 300 °C. A large amount of N_2O was detected with a maximum yield of 41% at 250 °C. Taking into account the high reducibility of $LaFe_{0.94}Pd_{0.06}O_3$ found by H_2-TPR (Fig. 1), the great performance of the Pd-containing sample for NO removal at low temperature was attributed to its excellent redox properties, which can initiate the redox reaction with a small energy barrier.

4.6. The influence of O_2 in feed on the catalytic behavior of $LaFe_{0.8}Cu_{0.2}O_3$

A serious inhibiting effect of O_2 was observed during the reaction of 3000 ppm NO and 3000 ppm CO over $LaFe_{0.8}Cu_{0.2}O_3$ (Figs. 7a–7d). The N_2 yield and N_2O concentration were severely depressed by 500 ppm O_2. In the presence of 5% O_2, N_2 yield was essentially inhibited with values below 6%. In contrast, a remarkable improvement in CO conversion was obtained with the O_2 in the feed. Significant NO_2 generation was observed at 5% O_2. The corresponding ratio of X_{NO}/X_{CO} under different O_2 feed concentrations as a function of temperature is plotted in Fig. 9, showing that X_{NO}/X_{CO} values diminished with increasing O_2 concentration and were much lower than 1 in the presence of 5% O_2 at 200 °C. Above 400 °C, a slight decline in X_{NO}/X_{CO} was observed, possibly correlated with the inhibition of NO oxidation to NO_2 by 5% O_2 (see Fig. 7c) due to the unfavorable thermal equilibrium for this reaction at high temperature. The above results strongly imply that the reaction was totally controlled by the unfavorable oxidation of the reducing agent CO, as formulated in Eq. (9) with 5% O_2. At 500 ppm O_2, the X_{NO}/X_{CO} values increased progressively up to 0.59 as the reaction temperature increased from 200 to 500 °C, revealing a competitive reaction between NO reduction by CO with CO oxidation by O_2. It seems that the percentage of NO reduction increased gradually at elevated temperature.

5. Conclusion

Nanoscale $LaFe_{1-x}(Cu, Pd)_xO_3$ perovskites were prepared by reactive grinding with specific surface areas above 30 m^2/g, even after calcination at 500 °C for 5 h, and crystal domain sizes below 20 nm. More anion vacancies were generated after Cu^{2+} partial substitution of Fe^{3+} ions in the B sites of the lattice due to a positive charge deficiency. The nitrosyl species formed via NO chemical adsorption on these anion vacancies was highly reactive toward CO according to TPSR experiments. On the

other hand, Cu substitution also enhanced the reducibility of lanthanum ferrite and accelerated the regeneration of anion vacancies on the surface. Therefore, a significant improvement in catalytic performance of NO + CO reaction was achieved over $LaFe_{0.8}Cu_{0.2}O_3$ compared with $LaFeO_3$.

The reducibility of $LaFeO_3$ was remarkably enhanced after incorporation of Pd into the lattice, resulting in a reduction peak at a temperature as low as 78 °C. This outstanding redox characteristic of $LaFe_{0.97}Pd_{0.03}O_3$ led to great performance for NO reduction and CO oxidation at low temperatures.

At low temperatures, the chemisorbed NO (nitrosyl species) was dissociated over perovskites with the formation of both N_2 and N_2O, as well as an oxidized surface. This oxidized surface subsequently can be reduced by CO with regeneration of anion vacancies for the continuous reaction. N_2O was further reduced by CO, and this transformation became pronounced with increasing temperature.

NO decomposition was difficult over $LaFe_{0.8}Cu_{0.2}O_3$ at temperatures below 500 °C. In contrast, N_2O could be decomposed at $T > 350$ °C, achieving a N_2 yield of 31% at 500 °C and 50,000 h^{-1} GHSV. Nevertheless, both NO and N_2O transformations were obviously promoted in the presence of CO.

O_2 strongly inhibited N_2 yield by suppressing the reducing agent through unfavorable CO oxidation. As a result, the reaction of NO and CO in the presence of 5% O_2 was controlled by CO oxidation.

NO reduction was previously studied over the same catalysts but using propene as a reducing agent and in the presence of oxygen [13], suggesting that NO reduction proceeded involving NO_3^- species over the surface. However, the conclusion obtained in the present work shows that nitrosyl species (NO^-) is the main adsorbed reactant participating in the NO reduction by CO [Eqs. (10) and (11)]. The higher efficiency of CO (compared with propene) in reducing the perovskite surface [Eqs. (7)–(9)] explains the difference between these two systems.

The surface concentration of O_2^- species in the presence of propene and oxygen was higher (compared with CO alone), thus resulting in a higher NO_3^- density over the surface. This nitrate species was subsequently reduced by propene. The surface density of nitrosyl species was lower (again compared with CO in the gas phase), and nitrosyl species was also inactive toward propene. The NO catalytic reduction mechanisms with these two reducing agents were accordingly different.

Acknowledgments

Financial support of NSERC through its industrial chair program is gratefully acknowledged. The authors thank Nanox Inc. for the preparation of the perovskite samples.

References

[1] M.L. Rojas, J.L.G. Fierro, L.G. Tejuca, A.T. Bell, J. Catal. 124 (1990) 41.
[2] L. Lisi, G. Bagnasco, P. Ciambelli, S. De Rossi, P. Porta, G. Russo, M. Turco, J. Solid State Chem. 146 (1999) 176.
[3] G. Parravano, J. Chem. Phys. 20 (1952) 342.
[4] W.F. Libby, Science 171 (1971) 499.
[5] A.E. Giannakas, A.K. Ladavos, P.J. Pomonis, Appl. Catal. B 49 (2004) 147.
[6] A.A. Leontiou, A.K. Ladavos, P.J. Pomonis, Appl. Catal. A 241 (2003) 133.
[7] V.C. Belessi, C.N. Costa, T.V. Bakas, T. Anastasiadou, P.J. Pomonis, A.M. Efstathiou, Catal. Today 59 (2000) 347.
[8] S.D. Peter, E. Garbowski, V. Perrichon, M. Primet, Catal. Lett. 70 (2000) 27.
[9] F. Garin, L. Simonot, G. Maire, Appl. Catal. B 11 (1997) 181.
[10] S.D. Peter, E. Garbowski, V. Perrichon, B. Pommier, M. Primet, Appl. Catal. A 205 (2001) 147.
[11] M. Iwamoto, H. Yahiro, T. Kutsuno, S. Bunyu, S. Kagawa, Bull. Chem. Soc. Jpn. 62 (1989) 583.
[12] Y. Wan, J.X. Ma, Z. Wang, W. Zhou, S. Kaliaguine, J. Catal. 227 (2004) 242.
[13] R.D. Zhang, A. Villanueva, H. Alamdari, S. Kaliaguine, J. Catal. 237 (2006) 368.
[14] R.D. Zhang, A. Villanueva, H. Alamdari, S. Kaliaguine, Appl. Catal. B 64 (2006) 220.
[15] R.D. Zhang, A. Villanueva, H. Alamdari, S. Kaliaguine, Appl. Catal. A 307 (2006) 85.
[16] N. Guilhaume, S.D. Peter, M. Primet, Appl. Catal. B 10 (1996) 325.
[17] Y. Nishihata, J. Mizuki, T. Akao, H. Tanaka, M. Uenishi, M. Kimura, T. Okamoto, N. Hamada, Nature 418 (2002) 164.
[18] Y.-H. Chin, W.E. Alvarez, D.E. Resasco, Catal. Today 62 (2000) 291.
[19] M. Crespin, W.K. Hall, J. Catal. 69 (1981) 359.
[20] S. Kaliaguine, A. Van Neste, Process for synthesizing perovskites using high energy milling, U.S. patent 6017504, 2000.
[21] J. Shu, S. Kaliaguine, Appl. Catal. B 16 (1998) L303.
[22] S. Kaliaguine, A. van Neste, V. Szabo, J.E. Gallot, M. Bassir, R. Muzychuk, Appl. Catal. A 209 (2001) 345.
[23] V. Szabo, M. Bassir, A. van Neste, S. Kaliaguine, Appl. Catal. B 43 (2003) 81.
[24] S. Royer, A. van Neste, R. Davidson, S. McIntyre, S. Kaliaguine, Ind. Eng. Chem. Res. 43 (2004) 5670.
[25] S. Varma, B.N. Wani, N.M. Gupta, Appl. Catal. A 241 (2003) 341.
[26] P. Ciambelli, S. Cimino, L. Lisi, M. Faticanti, G. Minelli, I. Pettiti, P. Porta, Appl. Catal. B 33 (2001) 193.
[27] P. Porta, S. Cimino, S. de Rossi, M. Faticanti, G. Minelli, I. Pettiti, Mater. Chem. Phys. 71 (2001) 165.
[28] W.J. Shen, M. Okumura, Y. Matsumura, M. Haruta, Appl. Catal. A 213 (2001) 225.
[29] L.G. Tejuca, J.L.G. Fierro, J.M.D. Tascón, Adv. Catal. 36 (1989) 237.
[30] T. Seiyama, N. Yamazoe, K. Eguchi, Ind. Eng. Chem. Prod. Res. Dev. 24 (1985) 19.
[31] L.A. Isupova, A.A. Budneva, E.A. Paukshtis, V.A. Sadykov, J. Mol. Catal. A 158 (2000) 275.
[32] E. Giamello, D. Murphy, G. Magnacca, C. Morterra, Y. Shioya, T. Nomura, M. Anpo, J. Catal. 136 (1992) 510.
[33] G. Centi, S. Perathoner, Appl. Catal. A 132 (1995) 179.
[34] X. She, M. Flytzani-Stephanopoulos, J. Catal. 237 (2006) 79.
[35] B. Coq, D. Tachon, F. Figuéras, G. Mabilon, M. Prigent, Appl. Catal. B 6 (1995) 271.
[36] S. Shin, H. Arakawa, Y. Hatakeyama, K. Ogawa, K. Shimomura, Mater. Res. Bull. 14 (1979) 633.
[37] V.A. Matyshak, O.V. Krylov, Catal. Today 25 (1995) 1.
[38] J.M.D. Tascón, L.G. Tejuca, C.H. Rochester, J. Catal. 95 (1985) 558.
[39] R.J.H. Voorhoeve, Advanced Materials in Catalysis, New York, 1977, p. 129.
[40] B. Viswanathan, Catal. Rev.-Sci. Eng. 34 (1992) 337.
[41] M.W. Chien, I.M. Pearson, K. Nobe, Ind. Eng. Chem. Prod. Res. Dev. 14 (1975) 131.
[42] C. Shi, M. Cheng, Z. Qu, X. Yang, X. Bao, Appl. Catal. B 36 (2002) 173.
[43] Y. Teraoka, H. Fukuda, S. Kagawa, Chem. Lett. (1990) 1.
[44] H. Yasuda, N. Mizuno, M. Misono, J. Chem. Soc. Chem. Commun. (1990) 1094.

[45] C. Tofan, D. Klvana, J. Kirchnerova, Appl. Catal. A 223 (2002) 275.
[46] L. Forni, C. Oliva, T. Barzetti, E. Selli, A.M. Ezerets, A.V. Vishniakov, Appl. Catal. B 13 (1997) 35.
[47] J. Valyon, W.K. Hall, J. Phys. Chem. 97 (1993) 1204.
[48] H.X. Dai, H. He, P.H. Li, L.Zh. Gao, C.-T. Au, Catal. Today 90 (2004) 231.
[49] P.J. Gellings, H.J.M. Bouwmeester, Catal. Today 12 (1992) 1.
[50] V.C. Belessi, P.N. Trikalitis, A.K. Ladavos, T.V. Bakas, P.J. Pomonis, Appl. Catal. A 177 (1999) 53.